Control of Independent-Input, Parallel-Output DC/DC Converters for Modular Battery Building Blocks

Mohamed Kamel*, M. Muneeb Ur Rehman*, Fan Zhang**, Regan Zane* and Dragan Maksimovic**
*Electrical and Computer Engineering, Utah State University
Logan, Utah – USA 84341
Email: mohahmedkamel@aggiemail.usu.edu
**Electrical, Computer and Energy Engineering, University of Colorado Boulder
Boulder, Colorado – USA 80309

***Abstract*—Modular battery packs are desirable energy storage elements in applications such as DC microgrids and electric vehicles (EVs). Modular battery packs utilize DC/DC converters that are connected in series for high output voltage or connected in parallel for high output currents. An active battery management system (BMS) utilizes the cell state of charge (SOC) to control the cell current. The individual control to input current transfer functions vary with the number of converters in parallel. This paper presents a small-signal model for the parallel converters as a multi-input, multi-output (MIMO) system that shows the interactions among the input current transfer functions. The small-signal model is utilized to design the feedback loop. The paper uses hybrid feedforward control to reduce the interactions between the coupled input-current regulation loops; which simplifies the implementation, increases modularity, and eliminates the need for a central controller. that is generally employed in MIMO systems. The analysis is verified by simulations and by experiments. A 300 W module consisting of three parallel output 100 W boost converters for a cell active balancing management system is used for hardware validation.**

Keywords—BMS, active balancing, decoupling control, parallel converters, IIPO, hybrid feedforward.

I. INTRODUCTION

Modular battery system architectures have benefits of scalability, improved reliability, and advanced active balancing features [1-7]. This paper is focused on the independent-input, parallel-output (IIPO) active balancing architecture, as shown in Fig. 1. In IIPO, the battery cells share the same output voltage at the point of interconnection (POI) and share part of the output current based on battery balancing objectives [8-10]. The IIPO approach allows paralleling battery bricks (modules) with different capacity or in some cases different chemistry via DC/DC converters. An active battery management system (BMS) controls the individual cell currents to equalize battery SOCs according to the system objectives [9-10].

In an IIPO module, each DC/DC converter utilizes a compensator to regulate the cell (input) current. For a DC/DC converter supplying a fixed load, the design of the current compensator depends on the uncompensated loop gain of the converter. However, because of paralleling, the control to input current transfer function varies with the numbers of DC/DC converters, which comes from the cross-coupling terms (off-diagonal) in the small-signal model. In addition, the cross-coupling terms introduce additional disturbances in the different current loops when the BMS changes an individual cell current reference of a specific converter. It is essential to understand the correlation between battery current and duty cycle of other converters for the control of the IIPO system. In MIMO systems such as the IIPO, decoupling control has been used to diagonalize the transfer function matrix, which theoretically cancels the cross-coupling effects. For N converters, the size of the decoupling matrix is a square matrix of order N [11, 15-16]. The decoupling terms can be high order transfer functions that are computationally complex for implementation on low-cost microcontrollers. References [13, 18] use the Relative Gain Array (RGA) approach, where the RGA matrices are evaluated at DC to decouple the steady-state interactions for computational simplicity. However, since both methods require accurate small-signal models of the system, these two approaches are not suitable for the IIPO systems in the active BMS applications where the loads and cell voltages vary frequently.

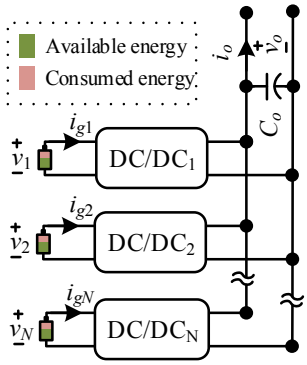

Fig. 1. Independent-input, parallel-output (IIPO) battery building block (module)

This paper presents a small-signal model of the IIPO module and proposes a hybrid feedforward control strategy for the individual input current control. The proposed approach

The information, data, or work presented herein was sponsored in part by the Department of the Navy, Office of Naval Research.

develops a feedforward path for disturbance rejection in transients to reduce the disturbance recovery time in the input current control loops due to the interactions. The paper is organized as follows. Section II describes the differences in the control to input current transfer functions of a single converter operating at its rated power and two IIPO converters each operating at rated power. Section III explains the coupling effects on the feedback loop and presents analysis of the hybrid feedforward compensator. Section IV verifies the control approach using time domain simulations in PLECS/MATLAB. Experimental validation is given in Section V. Section VI concludes the paper.

II. Small Signal Analysis

Figure 2 shows a battery building block (module) that consists of two-IIPO boost converters operating at switching frequency f_s, where R_s is the parasitic resistance of the inductance L, C_o is the lumped output capacitance, R_L is the load resistance, i_o is the load current, v_o is the output voltage, v_1 and v_2 are the input voltages of the two converters, i_1 and i_2 are the input currents of the two converters, the control (duty) variables for the two converters are d_1 and d_2, respectively. Control to input current transfer function of a single converter is derived in Subsection II.A. Control to input current transfer functions of the converter in the IIPO module is formulated in Subsection II.B.

Single boost converter

For a single boost converter in the two- converter IIPO system of Fig. 2, the averaged inductor voltage and capacitor current equations over a switching cycle are given in (1) and (2) below, where the output load is split between the two boost converters with $C_{o1} = 0.5C_o$, $R_{L1} = 2R_L$.

$$L\frac{di_1}{dt} = v_1 - i_1R_s - \acute{D}_1v_o, \tag{1}$$

$$C_{o1}\frac{dv_o}{dt} = \acute{D}_1i_1 - \frac{v_o}{R_{L1}}, \tag{2}$$

By applying perturbation and linearization around the DC equilibrium point (I_1, D, D', V_o, V_1) [22], the transfer functions (considering only the control variables) for a single boost converter are obtained in (3-5) as follows,

$$G_{id} = \frac{(V_o + \acute{D}_1I_1R_{L1}) + C_{o1}R_{L1}V_os}{Den_1(s)}, \tag{3}$$

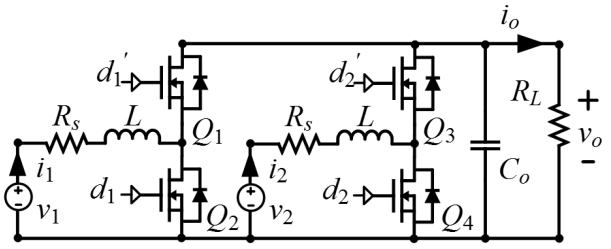

Fig. 2. One module – two IIPO boost converters

$$G_{vd} = \frac{(\acute{D}_1V_oR_{L1} - I_1R_{L1}R_s) - I_1R_{L1}Ls}{Den_1(s)}, \tag{4}$$

$$Den_1(s) = C_{o1}R_{L1}Ls^2 + (C_{o1}R_{L1}R_s + L)s + R_s + \acute{D}_1^2R_{L1}. \tag{5}$$

A. Two IIPO boost converters

Deriving a complete small-signal model for the system is a lengthy process, which depends on the number of battery cells and converters [11-14]. The presented analysis ignores the circulation currents that are discussed in [23]. This analysis relies on averaging the two inductor voltages and the output capacitor current over a full switching interval as given in (6-7). By applying perturbation and linearization around the DC equilibrium point (I_1, I_2, D_1, D'_1, D_2, D'_2, V_o, V_1, V_2) [22], the transfer functions (considering only the control variables) for the two IIPO boost converters can be derived as

$$L\frac{di_1}{dt} = v_1 - i_1R_s - \acute{D}_1v_o, \tag{6}$$

$$L\frac{di_2}{dt} = v_2 - i_2R_s - \acute{D}_2v_o, \tag{7}$$

$$C_o\frac{dv_o}{dt} = \acute{D}_1i_1 + \acute{D}_2i_2 - \frac{v_o}{R_L}, \tag{8}$$

$$\begin{bmatrix}\tilde{i}_1\\ \tilde{i}_2\\ \tilde{v}_o\end{bmatrix} = \begin{bmatrix}g_{11} & g_{12}\\ g_{21} & g_{22}\\ g_{vd1} & g_{vd2}\end{bmatrix}\begin{bmatrix}\tilde{d}_1\\ \tilde{d}_2\end{bmatrix} = \begin{bmatrix}G_{imat2x2}\\ G_{vmat1x2}\end{bmatrix}\begin{bmatrix}\tilde{d}_1\\ \tilde{d}_2\end{bmatrix}, \tag{9}$$

where, g_{11} is the transfer function from the perturbations $\tilde{d}_1$ to current $\tilde{i}_1$, g_{12} is the transfer function from the perturbations $\tilde{d}_2$ to current $\tilde{i}_1$, g_{21} is the transfer function from the perturbations $\tilde{d}_1$ to current $\tilde{i}_2$, g_{22} is the transfer function from the perturbations $\tilde{d}_2$ to current $\tilde{i}_2$, g_{vd1} is the transfer function from the perturbations $\tilde{d}_1$ to voltage $\tilde{v}_o$, g_{vd1} is the transfer function from the perturbations $\tilde{d}_2$ to voltage $\tilde{v}_o$. $G_{imat2x2}$ is a control to input current transfer matrix consisting of the control to input current transfer functions. Detailed expressions for the transfer functions in (9) are summarized in Table I. A multitone analysis in PLECS/MATLAB is used to verify the expressions given in (3) and (9). The parameters of the switching model are summarized in Table II. Fig. 3 shows Bode plots of the control to input current transfer functions obtained in (3) and (9). In Fig. 3(a), the blue and red lines verify the analytically derived transfer function g_{11} and simulation results, respectively. Figure 3(a) clearly shows the difference in frequency response between the control to input current transfer function of a single boost converter and the control to input current transfer function of the significant magnitude response from the cross-coupling transfer function g_{12}, which invalidates SISO-based controller design approach based on a single converter transfer function (G_{id}).

TABLE. I: SMALL SIGNAL SUMMARY OF TWO-IIPO BOOST CONVERTERS

g_{11}	$\frac{C_oLV_oR_Ls^2+(LV_o+LR_L\acute{D}_1I_1+R_sV_oC_oR_L)s+R_sV_o+R_sR_L\acute{D}_1I_1+R_LV_o\acute{D}_2^2}{Den_{2x2}(s)}$
g_{12}	$\frac{LR_L\acute{D}_1I_2s-R_L\acute{D}_1(\acute{D}_2V_o-I_2R_s)}{Den_{2x2}(s)}$
g_{21}	$\frac{LR_L\acute{D}_2I_1s-R_L\acute{D}_2(\acute{D}_1V_o-I_1R_s)}{Den_{2x2}(s)}$
g_{22}	$\frac{C_oLV_oR_Ls^2+(LV_o+LR_L\acute{D}_2I_2+R_sV_oC_oR_L)s+R_sV_o+R_sR_L\acute{D}_2I_2+R_LV_o\acute{D}_1^2}{Den_{2x2}(s)}$
g_{vd1}	$\frac{-I_1L^2R_Ls^2+LR_L(\acute{D}_1V_o-2I_1R_s)s+R_sR_L(\acute{D}_1V_o-I_1R_s)}{Den_{2x2}(s)}$
g_{vd2}	$\frac{-I_2L^2R_Ls^2+LR_L(\acute{D}_2V_o-2I_2R_s)s+R_sR_L(\acute{D}_2V_o-I_2R_s)}{Den_{2x2}(s)}$
$Den_{2x2}(s)$	$C_oL^2R_Ls^3+(L^2+2C_oLR_sR_L)s^2+\left(LR_L\left(\acute{D}_1^2+\acute{D}_2^2\right)+R_s(C_oR_sR_L+2L)\right)s+R_s\left(R_L\left(\acute{D}_1^2+\acute{D}_2^2\right)+R_s\right)$

TABLE.II SWITCHING MODEL PARAMETERS

Parameter	Symbol	Value
Input voltages [V]	V_1, V_2	4
Output voltage [V]	Vo	4.8
Load power [W]	P_o	200
Output capacitor [μF]	C_o	240
Inductance [nH]	L	320
Parasitic resistance [mΩ]	R_s	5
Switching frequency [kHz]	f_s	200

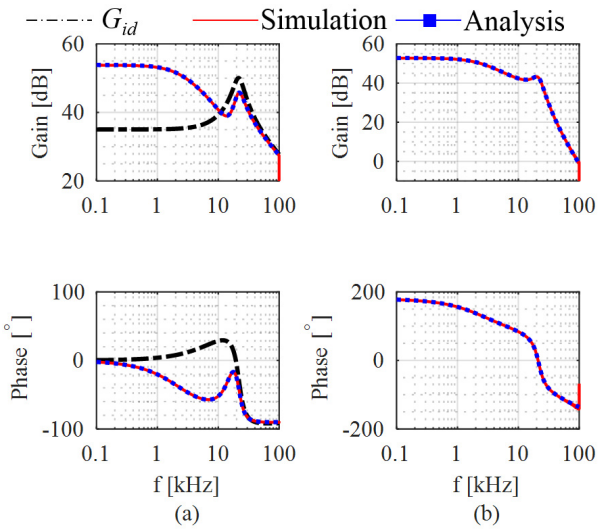

Fig. 3: Bode diagrams of control to input current transfer functions. In both (a) and (b) the blue and red lines verify the expressions for $g11$ and $g12$ by simulation. In (a) a comparison between G_{id}, and g_{11}. In (b) the frequency response of the cross-coupling transfer function g_{12}.

III. INPUT CURRENT REGULATION

Section II shows how the control to input current transfer function of a single boost converter changes in an IIPO module. It also shows the significance of the cross-coupling transfer function. This section considers $G_{imat2x2}$ in (9) as a classical Two-input, two-output (TITO) control problem [14,15]. In subsection III.A the cross-coupling effects on the feedback loop are discussed. Subsection III.B discusses the hybrid feedforward approach.

A. Feedback loop

By considering only the control variables in the closed loop-model [17] shown in Fig. 4, the closed-loop transfer function can be obtained by solving (9), (10), and (11),

$$\tilde{d}_1=G_{ci}(\tilde{i}_{ref\,1}-\tilde{i}_1)\,, \tag{10}$$

$$\tilde{d}_2=G_{ci}(\tilde{i}_{ref\,2}-\tilde{i}_2)\,, \tag{11}$$

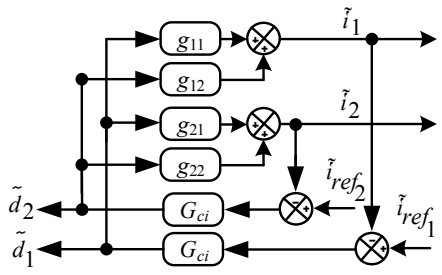

Fig. 4: Closed loop model considering only the control variables. The effects of input voltages and the output impedance are not shown in this Figure

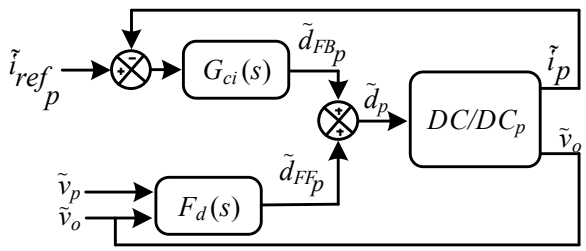

Fig. 5: Proposed hybrid feedofrward control for input current regulation

where G_{ci} is the current loop compensator, $\tilde{i}_{ref1}$ and $\tilde{i}_{ref2}$ are the perturbations on the current references for the two input currents. The solution for $\tilde{i}_1$ is given by

$$\tilde{i}_1 = \frac{G_{ci}(g_{11} + G_{ci}(g_{11}\,g_{22} - g_{12}\,g_{21}))\tilde{i}_{ref1} + G_{ci}g_{12}\tilde{i}_{ref2}}{G_{ci}(g_{11} + g_{22} + G_{ci}(g_{11}\,g_{22} - g_{12}\,g_{21})) + 1}. \quad (12)$$

Equation (12) shows that the characteristic equation depends on the diagonal elements and the determinant of $G_{imat2x2}$, and it shows that changing the reference of one converter is seen as a disturbance on the other converter. Designing a decoupling matrix for the system is cumbersome given the expressions for $G_{imat2x2}$ elements. The transfer matrix $G_{imat2x2}$ changes with the operating point and the cell SOC. Furthermore, such decoupling control techniques [13,18] require centralized and sophisticated signal processing. Although the existing battery management systems are centralized, the computational complexity, high cost, and size are typical drawbacks. The computational complexity of the active battery management system affects the available sampling rate and the feasibility of the implementation using low-cost microcontrollers. Consequently, the feedback compensator bandwidth may be limited to frequencies below the resonant frequency of the system. Without enough attenuation beyond the crossover frequency, any disturbance on the DC bus propagates in all control loops.

B. Hybrid feedforward control

Feedforward control utilizes the large signal model to calculate the control command, which is the duty-cycle of the converter. Hybrid feedforward control has been employed in the control of PWM converters. In [17], a voltage feedforward term was added to the current setpoint of the average current loop in the input-series output-parallel architecture to account for the input voltage mismatch of the different modules supplied by the same voltage source. In [19-21], the feedback and feedforward loops worked together for voltage regulation. The feedforward path in a hybrid feedforward compensation improves the input port stability at high frequency [24]. Figure 5 shows a feedback loop that relies on a compensator G_{ci} for input current regulation; the feedforward stage $F_d(s)$ utilizes the input voltage and the POI voltage measurement. The feedforward path depends on the conversion ratio of the DC/DC converter. In this paper, the DC/DC converters utilize synchronous rectification so that the system always operates in CCM. The control command is the superposition of the feedback $\tilde{d}_{FB}$ and feedforward $\tilde{d}_{FF}$ paths. The cell voltages change slowly; a relatively large bus capacitance damps the variations in the output voltage. As a result, the feedforward term dominates the duty-cycle. The feedforward term works on changing the duty cycle (D) as the output voltage (V_o) varies to maintain zero average voltage across the inductor. Consequently, the transient period vanishes quickly, which overcomes the extended period the converter would have had to undergo to track the original current reference before the disturbance instant at the POI. The controller works on finding the duty at which the steady-state equilibrium is achieved. In an ideal boost converter operating in CCM, the following expression can be found

$$V_p = \acute{D}_p V_o\,, \quad (13)$$

where, V_p is the input voltage, V_o is the output voltage, and $\acute{D}_p$ is compliment of the converter duty-cycle. By including perturbations around the DC operating point, (13) is written as

$$\tilde{d}_p = \frac{\acute{D}_p}{V_o}\tilde{v}_o - \frac{1}{V_o}\tilde{v}_p\,, \quad (14)$$

where, $\tilde{v}_p$ is the perturbation on the input voltage, $\tilde{v}_o$ is the perturbation on the output voltage, and $\tilde{d}_p$ is the perturbation on the control command. Equation (14) can be rewritten in the following form

$$\tilde{d}_{FFp} = X_p\,\tilde{v}_o - Y_p\,\tilde{v}_p\,, \quad (15)$$

where, X_p, and Y_p are scaling factors; if X_p and Y_p are chosen to be $\frac{\acute{D}_p}{V_o}$ and $\frac{1}{V_o}$, (15) and (14) are identical. For the analysis, define two matrices G_{v1}, and G_{v2} as in (16) and (17), respectively.

$$G_{v1} = \begin{bmatrix} g_{11} & g_{12} \\ g_{vd1} & g_{vd2} \end{bmatrix}. \quad (16)$$

$$G_{v2} = \begin{bmatrix} g_{21} & g_{22} \\ g_{vd1} & g_{vd2} \end{bmatrix}. \quad (17)$$

By combining the feedback path (10) and (11) with the feedforward path (15), a new hybrid feedforward closed-loop equation is obtained by solving (9), (18), and (19) for $\tilde{i}_1$, $\tilde{i}_{ref1}$, and $\tilde{i}_{ref2}$ as

$$\tilde{d}_1 = G_{ci}(\tilde{i}_{ref1} - \tilde{i}_1) + X_1\,\tilde{v}_o - Y\tilde{v}_1, \quad (18)$$

$$\tilde{d}_2 = G_{ci}(\tilde{i}_{ref2} - \tilde{i}_2) + X_2\,\tilde{v}_o - Y\tilde{v}_2, \quad (19)$$

$$\tilde{i}_1 = \frac{T_{F1}\tilde{i}_{ref1} + T_{F2}\,\tilde{i}_{ref2}}{1 + T_{FBFF}}, \quad (20)$$

$$T_{FB} = G_{ci}(g_{11} + g_{22} + G_{ci}(g_{11}g_{22} - g_{12}g_{21})), \quad (21)$$

$$T_{FBFF} = T_{FB} + G_{ci}(X_1|G_{v2}| - X_2|G_{v1}|) - X_1 g_{vd1} - X_2 g_{vd2}, \quad (22)$$

$$T_{F1} = G_{ci}\big(g_{11} + G_{ci}|G_{imat2x2}| - X_2|G_{v1}|\big), \quad (23)$$

$$T_{F2} = G_{ci}\left(g_{12} + X_1|G_{v2}|\right). \quad (24)$$

The hybrid feedforward loop gain T_{FBFF} is the superposition of the feedback loop gain T_{FB} and the feedforward gain. Figure 6 compares the two loop gains for a standard PI compensator $G_{ci} = \frac{2}{s} + \frac{1}{1+2\pi*1000}$. This compensator achieves a crossover frequency of nearly 300 Hz with feedback only using (12). However, the introduction of the feedforward path increases the crossover frequency to nearly 1600 Hz at the expense of a reduced phase margin. The feedforward dominates at higher frequencies and provides larger attenuation beyond the crossover frequency compared to feedback loop only. Although the feedback compensator may be designed for higher bandwidth, it may not provide sufficient attenuation at frequencies beyond the crossover frequency. Thus, the feedforward path can provide larger attenuation to DC bus disturbances that occur at frequencies beyond the compensator bandwidth.

IV. Simulation Results

For the two IIPO boost converters with the parameters listed in Table II, two simulations were carried out, using PLECS/MATLAB. One applies only feedback loop, and the other one uses the hybrid feedforward controller described in Section III. In the two scenarios, the two input currents are regulated at rated load. At certain point, the BMS applies a step change on the reference current of one converter. Figure 7 shows the simulation results, where (a) presents the simulation results for the converter that experiences a step change in the current reference with feedback only or the hybrid feedforward control, and (b) shows the simulation results for the other converter. From Fig. 7, it can be observed that the input currents track their references using feedback controllers. However, the additional feedforward action reduces the settling times for the two converters significantly. Additionally, the disturbance on the converter that has a fixed reference is reduced in the hybrid feedforward case due to a more substantial attenuation at higher frequencies. Hence, the proposed hybrid feedforward approach is verified through simulations.

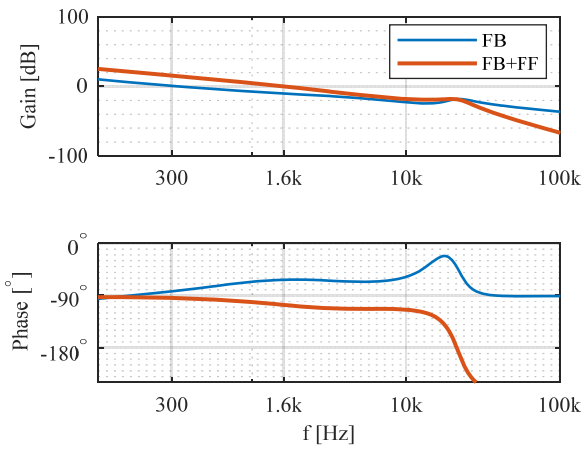

Fig. 6: Feedback and hybrid feedforward loop gain comparison

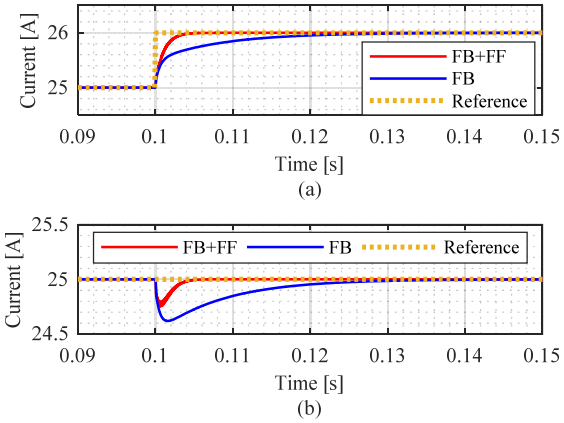

Fig. 7: Simulation results – (a) rererence tracking, (b) disturbance rejection

V. Experimental Validation

In this section, the proposed approach is validated using a module consisting of three battery cells and three boost converters in the IIPO configuration performing active battery management. As discussed in the previous sections, the control to input transfer matrix for such a system is of size 3. Similar to (12) for a two-converter system, a new characteristic equation is obtained for the three-converter system to enable design of the feedback compensator. The compensator takes the form $G_{ci} = \frac{1}{s} + \frac{1}{1+2\pi*3000}$. Figure. 8 shows an evaluation system for the IIPO active balancing system, where three DC/DC converters have independent 25 Ah NMC-battery cells connected to the converter inputs. The three converter outputs are paralleled to achieve higher output current. Single microcontroller (Piccolo TMS320F280049) hosts three input current compensators for cost reduction. A constant current load is used to draw 300 W from the common DC bus. Table III summarizes the hardware parameters. The ADC sampling rate is the same for the input

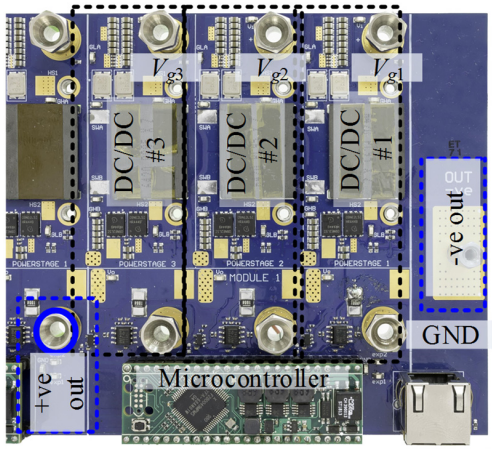

Fig. 8: Experimental prototype

current, input voltage, and output voltage sensing. The sampling rate is 10 kHz; in the implementation of the hybrid feedforward approach, the input and output voltages are low-pass filtered.

TABLE.III HARDWARE PARAMETERS

Parameter	Symbol	Value
Input voltages [V]	V_{g1}, V_{g2}, V_{g3}	~4
Output voltage [V]	Vo	~4.8
Output current [A]	Io	~60
Output capacitor [µF]	C_o	360
Switching frequency [kHz]	f_s	200
sampling rate [kHz]	f_{sam}	10

In the implementation of the feedback loop, the minimum duty command is zero. At that operating point, the input and the output voltages are the same. However, in the implementation of the hybrid feedforward approach, a negative saturation limit is applied on the output of the feedback compensator. The feedback compensator saturation limits in the hybrid feedforward approach are smaller than the feedback only implementation.

Figure 9 shows experimental results for the feedback only implementation. Initially, the three input currents are regulated at 26 A. The BMS applies a step change of +1 A on the current reference of I_{g3}. The input current I_{g3} tracks the new reference. Due to the disturbance in the DC bus coupling at the output, the input currents I_{g1} and I_{g2} slightly dip and spend a short time before they recover back to their old values. The recorded battery voltages are also shown, together with two cursor measurements.

Figure 10 shows experimental results for the hybrid feedforward control approach. Initially, the BMS issues a common current command of +26 A for the three input currents. Then, the BMS applies a step change of +1 A on the current reference for I_{g3}. Due to the difference in the SOCs of the three battery cells, the DC operating point with hybrid feedforward control is slightly different, which can be observed from the current trace of I_{g2}.

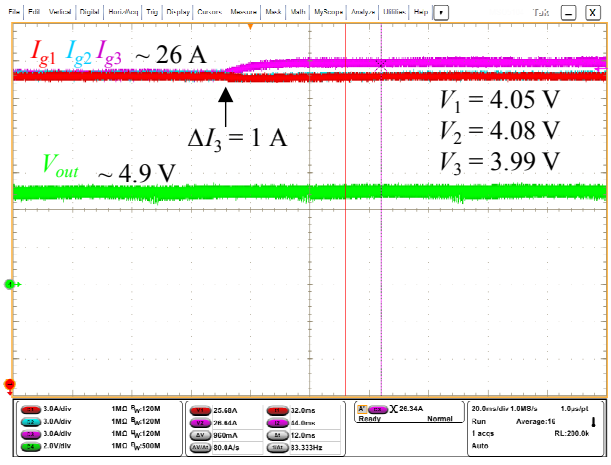

Fig. 9. Experimental results – feedback control

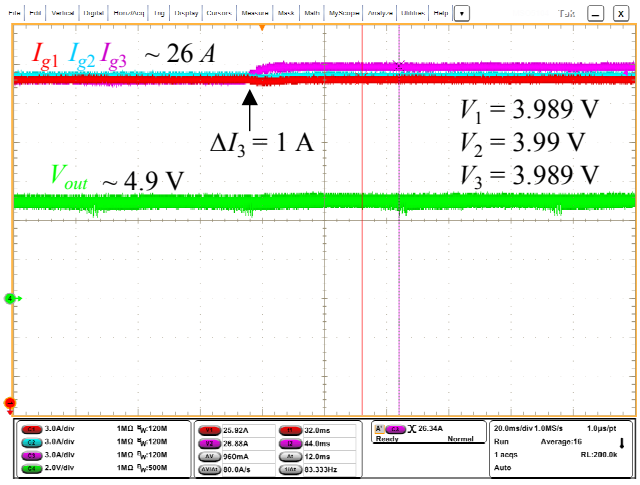

Fig. 10. Experimental results – hybrid feedforward control

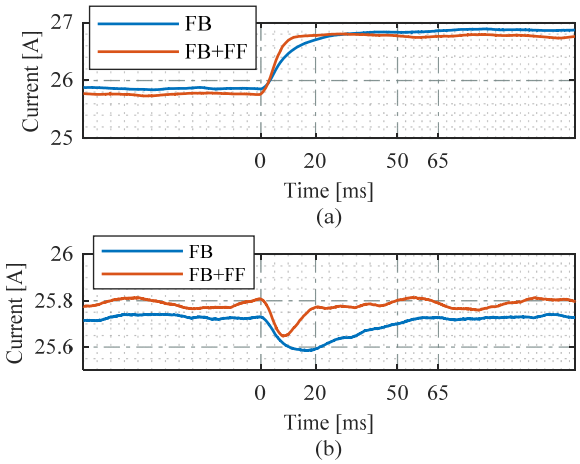

Fig. 11. Experimental results – comparison between feedback and hybrid feedbforward control – (a) DC/DC #3, (b) DC/DC #1

Figure 11 compares the experimental results from the feedback validation and the feedforward approach. To obtain the waveforms in Fig. 11, the current scope traces are low-pass filtered to remove the switching ripple from the waveforms.

Figure 11 (a) shows comparison between the step response of I_{g3} with feedback only and hybrid feedforward approach. There is a slight difference in the steady-state results between the two responses due to the variations in SOC. It can be observed that the hybrid feedforward response is faster. The current reaches a steady-state in approximately 20 msec. In contrast, the settling time with feedback only is about 50 msec.

Figure 11 (b) shows a comparison between the disturbance rejection of I_{g1} using feedback controller and with the hybrid feedforward approach. Delays due to filtering contribute to somewhat reduced phase margin, resulting in slightly increased oscillations in the response of the hybrid feedforward control. The response is also affected by duty cycle quantization effects. However, using hybrid feedforward control the current recovers

from the disturbance and returns to the regulation value in approximately 20 msec. With feedback control, the response time is approximately 50 msec, and the current undershoot is larger.

VI. Conclusion

This paper models the control to input current transfer functions of the independent-input, parallel-output (IIPO) DC/DC converters in modular battery building blocks. Analysis showing interactions of the different input current control loops is presented. Hybrid feedback plus feedforward control is proposed to deal with the bandwidth limitations due to coupling. Switching model simulations and a 300 W experimental prototype consisting of three parallel output 100 W boost converters and three (NMC) battery cells demonstrate the interactions between the different control loops and the effectiveness of the hybrid feedforward approach.

VII. References

[1] D. C. Hopkins, C. R. Mosling, and S. T. Hung, "Dynamic equalization during charging of serial energy storage elements," IEEE Transactions on Industry Applications, vol. 29, no. 2, pp. 363–368, Mar. 1993.

[2] C. S. Moo, K.-S. Ng, and J.-S. Hu, "Operation of battery power modules with series output," in 2009 IEEE International Conference on Industrial Technology, 2009, pp. 1–6.M.

[3] Y. Chen, X. Liu, Y. Cui, J. Zou, and S. Yang, "A MultiWinding Transformer Cell-to-Cell Active Equalization Method for Lithium-Ion Batteries with Reduced Number of Driving Circuits," IEEE Transactions on Power Electronics, vol. 31, no. 7, pp. 4916–4929, Jul. 2016.

[4] M. Evzelman, M. M. U. Rehman, K. Hathaway, R. Zane, D. Costinett, and D. Maksimovic, "Active Balancing System for Electric Vehicles with Incorporated Low-Voltage Bus," IEEE Transactions on Power Electronics, vol. 31, no. 11, pp. 7887–7895, Nov. 2016.

[5] Y. Li and Y. Han, "A Module-Integrated Distributed Battery Energy Storage and Management System," IEEE Transactions on Power Electronics, vol. 31, no. 12, pp. 8260–8270, Dec. 2016.

[6] D. F. Frost and D. A. Howey, "Completely Decentralized Active Balancing Battery Management System," IEEE Transactions on Power Electronics, vol. 33, no. 1, pp. 729–738, Jan. 2018.

[7] J.-W. Kim, J.-S. Yon, and B. H. Cho, "Modeling, control, and design of input-series-output-parallel-connected converter for high-speed-train power system," IEEE Transactions on Industrial Electronics, vol. 48, no. 3, pp. 536–544, Jun. 2001.

[8] M. Shousha, A. Prodić, V. Marten and J. Milios, "Design and Implementation of Assisting Converter-Based Integrated Battery Management System for Electromobility Applications," in IEEE Journal of Emerging and Selected Topics in Power Electronics, vol. 6, no. 2, pp. 825-842, June 2018.

[9] W. Chen, X. Ruan, H. Yan, and C. K. Tse, "DC/DC Conversion Systems Consisting of Multiple Converter Modules: Stability, Control, and Experimental Verifications," IEEE Transactions on Power Electronics, vol. 24, no. 6, pp. 1463–1474, Jun. 2009.

[10] Zhang, Fan, "Modeling and Control of a Modular Battery Management System for Lithium-ion Battery Packs" (2017). Electrical, Computer & Energy Engineering Graduate Theses & Dissertations. 153. https://scholar.colorado.edu/ecen_gradetds/153.

[11] Muneeb Ur Rehman, Muhammad, "Modular, Scalable Battery Systems with Integrated Cell Balancing and DC Bus Power Processing" (2018). All Graduate Theses and Dissertations. 6999. https://digitalcommons.usu.edu/etd/6999.

[12] Z. Qian, O. Abdel-Rahman, H. Al-Atrash, and I. Batarseh, "Modeling and Control of Three-Port DC/DC Converter Interface for Satellite Applications," IEEE Transactions on Power Electronics, vol. 25, no. 3, pp. 637–649, Mar. 2010.

[13] Zhang, Yu, "Small-Signal Modeling and Analysis of Parallel-Connected Power Converter Systems for Distributed Energy Resources"(2011). Open Access Dissertations. 551. https://scholarlyrepository.miami.edu/oa_dissertations/551.

[14] M. Veerachary, "Two-Loop Controlled Buck-SEPIC Converter for Input Source Power Management," IEEE Transactions on Industrial Electronics, vol. 59, no. 11, pp. 4075–4087, Nov. 2012.

[15] P. Wang, X. Lu, X. Yang, W. Wang, and D. Xu, "An Improved Distributed Secondary Control Method for DC Microgrids With Enhanced Dynamic Current Sharing Performance," IEEE Transactions on Power Electronics, vol. 31, no. 9, pp. 6658–6673, Sep. 2016.

[16] S. Skogestad and I. Postelthwaite, Multivariable Feedback Control: Analysis and Design, 2nd Edition, John Wiley & Sons, Inc., 2006.

[17] P, Albertos and S, Antonio, Multivariable Control Systems, Springer, 2006.

[18] D. O'Keeffe, S. Riverso, L. Albiol-Tendillo, and G. Lightbodyt, "Distributed hierarchical droop control of boost converters in DC microgrids," in 2017 28th Irish Signals and Systems Conference (ISSC), 2017, pp. 1–6.

[19] U. Anwar, H. Kim, H. Chen, R. Erickson, D. Maksimovic, and K. K. Afridi, "A high power density drivetrain-integrated electric vehicle charger," in 2016 IEEE Energy Conversion Congress and Exposition (ECCE), 2016, pp. 1–8.

[20] U. Anwar, D. Maksimović, and K. K. Afridi, "Generalized hybrid feedforward control of pulse width modulated switching converters," in 2016 IEEE 17th Workshop on Control and Modeling for Power Electronics (COMPEL), 2016, pp. 1–7.

[21] U. Anwar, D. Maksimović, and K. K. Afridi, "A simple control architecture for four-switch buck-boost converter based power factor correction rectifier," in 2017 IEEE 18th Workshop on Control and Modeling for Power Electronics (COMPEL), 2017, pp. 1–6.

[22] R. W. Erickson and D. Maksimović, Fundamentals of Power Electronics, Second Edi. Kluwer Academic Publishers, 2001.

[23] Y. Xia, M. Yu, Y. Peng and W. Wei, "Modeling and Analysis of Circulating Currents Among Input-Parallel Output-Parallel Nonisolated Converters," in IEEE Transactions on Power Electronics, vol. 33, no. 10, pp. 8412-8426, Oct. 2018.

[24] H. Y. Cho and E. Santi, "Modeling and stability analysis in multi-converter systems including positive feedforward control," 2008 34th Annual Conference of IEEE Industrial Electronics, Orlando, FL, 2008, pp. 839-844.